J. Fluid Mech. (1975), *vol.* 68, *part* 2, *pp.* 353–368
Printed in Great Britain

Numerical simulation of cellular convection in air

By N. F. VELTISHCHEV AND A. A. ŽELNIN
Hydrometeorological Centre of the U.S.S.R., Moscow

(Received 19 April 1974)

Three-dimensional convection in a Boussinesq fluid confined between horizontal rigid boundaries is studied in a series of numerical experiments. Convection in air, whose Prandtl number $Pr = 0{\cdot}71$, is systematically investigated, together with another model for $Pr = 1$. Convection with a steadily changing mean temperature is also considered. Two-dimensional rolls over the Rayleigh number range $4500 \leqslant Ra \leqslant 24000$ and three-dimensional flow patterns over the range $26000 \leqslant Ra \leqslant 32000$ are shown to be stable in air when the mean temperature of the layer is constant ($\partial\overline{T}/\partial t = \eta = 0$). Discrete changes in the slope of the heat-flux curve are shown to exist in the ranges

$$7000 \leqslant Ra \leqslant 8000, \quad 12000 \leqslant Ra \leqslant 14000 \quad \text{and} \quad 24000 \leqslant Ra \leqslant 26000$$

in air. Only the last discrete transition in the heat flux is associated with a significant transition in the flow pattern. Two-dimensional rolls with a horizontally asymmetric distribution of upward and downward motions over the range $4500 \leqslant Ra \leqslant 8000$, and three-dimensional flow patterns over the range $10000 \leqslant Ra \leqslant 20000$ are shown to be stable when the mean temperature varies with time. The circulation in a three-dimensional cell depends on the sign of the mean temperature change: downward motions occupy the centre of the cell when $\partial\overline{T}/\partial t > 0$, and upward motions when $\partial\overline{T}/\partial t < 0$. Motions start to be time dependent for $Ra > 20000$. Transitions in the planform are associated with discrete changes in the slope of the heat-flux curve. Transitions in both the heat flux and flow pattern depend quantitatively on the Prandtl number.

1. Introduction

In a horizontal convecting layer of fluid, a number of discrete transitions occur in both the flow pattern and heat flux before the flow becomes fully turbulent. These transitions have been recently studied both experimentally and theoretically. Most theoretical studies deal with the transitions in an infinite horizontal layer of fluid which is heated uniformly from below and cooled uniformly from above. There are two dimensionless parameters describing this problem. They are the Rayleigh number Ra and the Prandtl number Pr, defined as follows:

$$Ra = (g\alpha/\kappa\nu)\,\Delta T h^3, \quad Pr = \nu/\kappa,$$

where g is the acceleration due to gravity, d the thermal expansion coefficient, κ the thermal diffusivity, ν the kinematic viscosity, h the layer depth and ΔT the temperature difference across the layer.

In an experimental study with water and acetone Malkus (1954) discovered that the heat flux between horizontal plates varies in linear segments with the impressed temperature difference ΔT between the plates if their separation h and the fluid properties are maintained constant. The observations made by Willis & Deardorff (1967*b*) in air show an increase in the slope of the heat-flux curve at $Ra \simeq 8200$ and $Ra \simeq 24\,000$. Krishnamurti (1973) observed the first transition in air at $Ra = 5600$, but did not find the transition at $Ra = 8200$. She also pointed out that there are decreases in the slope of the heat-flux curve at $Ra \simeq 11\,000$ and $Ra \simeq 17\,000$. The observations by Brown (1973) in air show discrete transitions in the heat flux at $Ra \simeq 9600$ and $Ra \simeq 25\,000$.

In the observational studies by Willis & Deardorff (1967*a*, 1970), Krishnamurti (1973) and Brown (1973) it was noted that subjecting a horizontal layer of air to a slow increase in the Rayleigh number beyond the critical value led to the appearance of periodic fluctuations superimposed on two-dimensional rolls. Willis & Deardorff (1967*a*) observed temperature fluctuations beyond $Ra \simeq 6300$, and Brown (1973) beyond $Ra \simeq 6000$. The appearance of oscillatory motions in air at $Ra \simeq 5800$ was reported by Willis & Deardorff (1970) and at $Ra \simeq 5600$ by Krishnamurti (1973).

A theoretical study by Busse (1972) shows that in liquids with small Prandtl numbers two-dimensional rolls are unstable to oscillating three-dimensional disturbances as soon as the amplitude of the convective motions exceeds some critical value. A numerical simulation of three-dimensional convective motions in air by Somerville (1973) shows that at $Ra = 4000$ two-dimensional convective rolls are the steady pattern. At $Ra = 9000$ his model reproduces the experimentally observed unsteady equilibrium state of vertically coherent oscillatory waves superimposed on rolls.

In the present study three-dimensional calculations in air are extended to $Ra = 32\,000$ and compared with observational data.

The second task of this study was to simulate convective motions in a domain with a nonlinear conduction temperature profile. The influence of this factor was studied theoretically by Palm (1960), Segel & Stuart (1962), Segel (1965), Krishnamurti (1968*a*) and Veltishchev (1969). All these authors came to the same general conclusion that the hexagonal pattern can be steady at slightly supercritical Rayleigh numbers. This conclusion was supported by experiments of Krishnamurti (1968*b*). The finite amplitude analysis which was used in these studies is quite complete but restricted to relatively small supercritical Rayleigh numbers. The numerical simulation of convective motions in an internally heated fluid layer by Thirlby (1970) shows that hexagonal cells with downward motion in the centre are stable when $Pr = 6{\cdot}8$. In the case of small Prandtl number ($Pr = 1$) his model reproduces two-dimensional rolls.

In the present study numerical experiments are extended to the cases of a mean temperature steadily increasing or decreasing with time for small Prandtl numbers ($Pr = 0{\cdot}71$ and 1).

2. Governing equations and numerical method

The fluid is characterized by its mean density ρ_0 (except in the buoyancy term), coefficient of thermal expansion α, coefficient of kinematic viscosity ν and coefficient of thermometric conductivity κ, all assumed to be constant. A fluid layer of depth h and infinite horizontal extent is confined above and below by perfectly conducting rigid boundaries. An adverse temperature difference ΔT is maintained across. the layer. In the conduction state, the temperature profile is defined as in the study by Krishnamurti (1968*a*):

$$T_s - T_r = -\frac{\Delta T}{h} Z + \frac{\eta}{2\kappa}(Z^2 - \tfrac{1}{4}h^2), \tag{1}$$

where T_s is the static temperature and T_r is a reference static temperature equal to ηt, where $\eta = \partial \bar{T}/\partial t$ = constant. This represents the case in which the temperature at all points in the fluid is changing at the same rate as that at the boundaries, and the shape of the temperature profile is independent of time.

Non-dimensionalizing by using h as the length scale, h^2/ν as the time scale, ΔT as the temperature scale and $\rho_0 \nu^2/h^2$ as the pressure scale, we obtain dimensionless equations for the conservation of momentum, mass and thermodynamic energy in the form

$$d\mathbf{V}/dt = -\operatorname{grad} p + RaPr^{-1}T\mathbf{k} + \nabla^2 \mathbf{V}, \tag{2}$$

$$\operatorname{div} \mathbf{V} = 0, \tag{3}$$

$$dT/dt = w - NZw + Pr^{-1}\nabla^2 T, \tag{4}$$

where $\mathbf{V}$ is the velocity vector, P the pressure, T the temperature deviation from the static value, w the vertical component of velocity, Z the non-dimensional height, $\mathbf{k}$ the unit vertical vector, Ra and Pr the Rayleigh and Prandtl numbers defined above and $N = \eta h^2 \kappa^{-1} \Delta T^{-1}$ the dimensionless parameter characterizing the variation in the mean temperature with time.

In the calculations to be reported in this paper cyclic (periodic) boundary conditions were used at the side walls. The horizontal extent of the domain in the X direction was 2·34 times the depth and in the Y direction was 4·032 times the depth. The initial state consisted of the conductive solution plus a random perturbation of small amplitude added to the temperature field.

An adaptation of Chorin's (1968) method was used to solve the system (2)–(4). For the calculations reported below, the numbers of grid points in the X, Y and Z directions were 25, 25 and 9, respectively. The details of the numerical method are described in the paper by Veltishchev & Želnin (1973).

The non-dimensional parameters Pr and N and the initial conditions were fixed in each numerical experiment. The integration was started from the initial conditions at a given Ra_0, and continued until a final steady or equilibrium unsteady state was reached at this Ra_0. The pattern obtained at Ra_0 provided the initial conditions for integration at the next Rayleigh number $Ra_1 = Ra_0 + \Delta Ra$, and so on. Increments $\Delta Ra = 1000$ were chosen over the range

$$4500 \leqslant Ra \leqslant 10\,000 \quad \text{and} \quad \Delta Ra = 2000$$

Experiment	Ranges of parameters: $Ra \times 10^{-3}$	Pr	N	Planform of initial temperature disturbances
1	4·5–32	0·71	0	
2	4·5–20	1·0	0	Hexagons with negative temperature deviations in the centres
3	4·5–24	0·71	7·3–11·0	
4	4·5–20	1·0	8·0–11·8	
5	4·5–8	1·0	−8·0– −9·3	
6	4·5	1·0	0	Rectangles
7	4·5	1·0	8·0	Hexagons with positive temperature deviations in the centres
8	4·5	1·0	0	Random field

TABLE 1. List of numerical experiments

over the range $10\,000 \leqslant Ra \leqslant 32\,000$. The non-dimensional time step was variable, and changed automatically to fulfil computational stability conditions

The computer output consisted of the Nusselt number Nu and absolute maxima $|\mathscr{U}|_{\max}$, $|\mathscr{V}|_{\max}$ and $|\mathscr{W}|_{\max}$ of the velocity components in the X, Y and Z directions at every time step, the horizontal and vertical profiles of all variables, the resulting mean temperature profile $T_s + \bar{T}$ and the vertical distribution of both the Nusselt number and dimensionless convective heat flux at arbitrary time intervals for a given Ra before transition to the next Ra. Such a procedure permits a general analysis of computational results with very high time resolution and detailed analysis of the flow patterns with adequate time resolution.

Table 1 lists the numerical experiments. An experiment will sometimes be referred to by its number in table 1.

3. Results

Linear conduction temperature profile for $N = 0$

Heat flux and resulting temperature profile for $Pr = 0{\cdot}71$. A plot of the heat flux $H = NuRa$ *vs.* the Rayleigh number Ra is shown in figure 1. The experimental values of H obtained by Willis & Deardorff (1967*b*), Krishnamurti (1973) and Brown (1973) are plotted for comparison. It may be seen from this figure that the computed heat flux is systematically larger than the observed one, but approaches the observed values more closely than do two-dimensional computations with a fixed wavelength (Willis, Deardorff & Somerville 1972).

It is difficult to discern the transitions in the heat flux from this small-scale figure, so the values of $\partial H/\partial Ra$, which can be interpreted as an effective conductivity, were computed. Table 2 shows values of $\partial H/\partial Ra$ obtained from our computations and from experimental data of Willis & Deardorff (1967*b*), Krishnamurti (1973) and Brown (1973).

It may be seen from this table that the first transition in the computed heat flux, in the range $7000 \leqslant Ra \leqslant 8000$, is in relatively good agreement with the

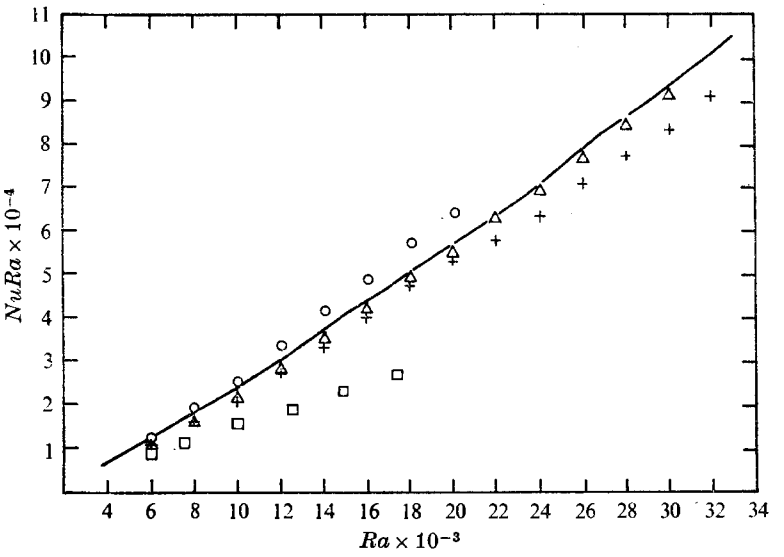

FIGURE 1. Heat flux $H = NuRa$ *vs.* Rayleigh number Ra for air ($Pr = 0{\cdot}71$, $N = 0$). ——, present numerical results; +, experiments by Willis & Deardorff (1967*b*); △, experiments by Brown (1973); □, experiments by Krishnamurti (1973); ○, two-dimensional computations with a fixed wavelength by Willis *et al.* (1972). Observational results for $Ra < 6000$ are not plotted owing to the scale of the figure.

transition observed by Willis & Deardorff (1967*b*), though later on it was considered doubtful by Willis *et al.* (1972) and Krishnamurti (1973). A second transition in the computed heat flux was obtained in the range

$$12\,000 \leqslant Ra \leqslant 14\,000$$

but was not observed in the experiments in air. The closest to it is a transition observed by Brown (1973) at $Ra = 9600$, but this seems to be too far from the computed one to be identified with it. The last computed transition, in $24\,000 \leqslant Ra \leqslant 26\,000$, closely agrees with that observed by Willis & Deardorff (1967*b*) and Brown (1973). As seen from this table the computed and observed values of the heat-flux slope are in a good agreement, but the positions of the boundaries between linear segments are sometimes quite different.

The values of the conductive (H_{cond}) and convective (H_{conv}) components of the heat flux across the convective layer have been computed, and values of $\partial H_{\mathrm{cond}}/\partial Ra$ and $\partial H_{\mathrm{conv}}/\partial Ra$ have been derived at each horizontal level of our domain. The computations show that both components of the heat flux have simultaneous transitions which correspond to transitions in the overall heat flux $H = NuRa$.

It is also worthwhile pointing out that transitions in the heat flux are associated with qualitative changes in the mean temperature profile. A positive temperature gradient was formed in the core of the convective layer after the first transition at $Ra = 8000$. The depth of this layer of positive temperature gradient doubled after the second transition at $Ra = 14\,000$, while the positive

$Ra \times 10^{-3}$	4·5	6	7	8	9	10	12	14	16	18	20	22	24	26	28	30	32	34	36
This study	2·68			2·86				3·25						3·50					
Willis and Deardorff (1967*b*)	1·87				3·18									3·50					
Brown (1973)	2·54 2·93							3·38 3·13						4·40 3·75					
Krishnamurti (1973)	1·37				1·60														

TABLE 2. Numerically and experimentally determined slopes $\partial H/\partial Ra$ for $Pr = 0{\cdot}71$, $N = 0$. Values in the first line are Rayleigh numbers used for the computations in this study. Slopes in the third and fourth lines were calculated from $Nu \times Ra$ curves in the original studies. The upper and lower values in the fourth line correspond to the slopes determined from figures 6(*a*) and (*b*) respectively in Brown's (1973) paper. The dashed line marks the upper limit of computations.

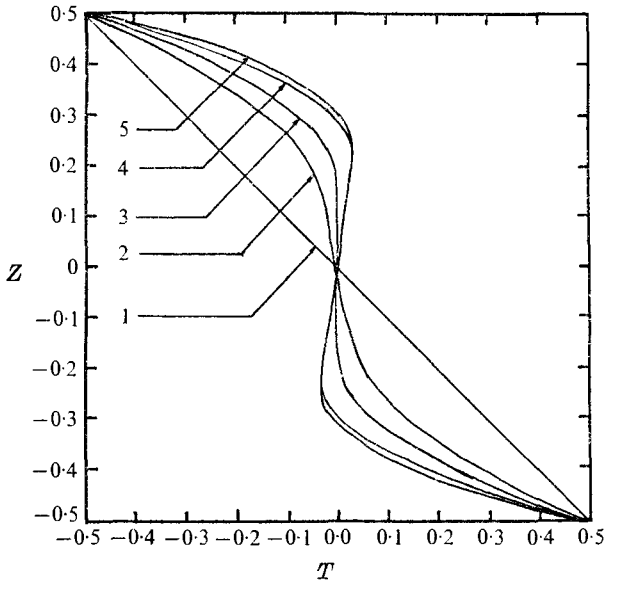

FIGURE 2. Mean temperature distribution (in non-dimensional units) across the convective layer at different Rayleigh numbers; $Pr = 0{\cdot}71$, $N = 0$. 1, undisturbed state; 2, $Ra = 4500$; 3, $Ra = 9000$; 4, $Ra = 20000$; 5, $Ra = 32000$.

temperature gradient tended to decrease after the third transition at $Ra = 26000$. With further increases in Ra the positive temperature gradient slowly increased again. Figure 2 shows mean temperature profiles at Rayleigh numbers corresponding to the middle of the linear segments of the heat-flux curve.

Flow and temperature patterns for $Pr = 0{\cdot}71$. Two-dimensional rolls were formed independently of the initial conditions at $Ra = 4500$. The differences were only in the orientation of the rolls and their wavelength. The aspect ratio (horizontal extent/depth) of our domain permits a maximum roll wavelength of 4·032. A wavelength close to the critical one was always selected. The relatively small aspect ratio of the computational domain is a weak point of this three-dimensional numerical simulation of convective motions, because only large discrete transitions in the wavelength are permitted. But at present it is hard to avoid these difficulties, since increasing the aspect ratio leads to an enormous increase in the computation time.

Thus a continuous increase in the horizontal wavelength with Ra as was observed in experiments could not be expected. Practically two-dimensional steady rolls with the same wavelength existed over the range $4500 \leqslant Ra \leqslant 24000$. A slight bimodality of the flow pattern appeared and increased progressively over the range $16000 \leqslant Ra \leqslant 32000$. At $Ra = 16000$ the amplitude of periodic motion, with wavelength close to the critical one, started to grow along the rolls, but an abrupt transition to a steady three-dimensional flow pattern occurred only at $Ra = 26000$, corresponding to the transition in the heat flux. An example of the horizontal distribution of vertical velocity in the middle of the convective layer at $Ra = 32000$ is shown in figure 3.

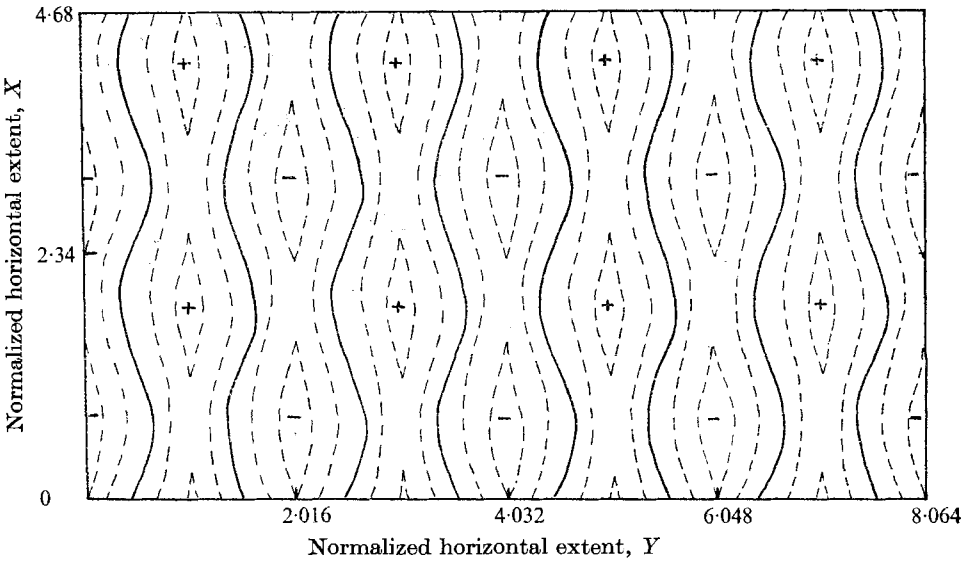

FIGURE 3. Horizontal distribution of vertical velocity in the middle of the convective layer at $Ra = 32000$ ($Pr = 0{\cdot}71$, $N = 0$). ——, zero vertical velocity; +, positions of maximum upward motion; −, positions of maximum downward motion. The original computational domain is repeated twice in both directions. Horizontal extents are normalized by the depth of the convective layer.

These results are at variance with both the experimental observations of Willis & Deardorff (1970) and Krishnamurti (1973) and the calculations of Somerville (1973) at $Ra = 9000$, which indicate oscillatory motions superimposed on two-dimensional rolls just after first the transition in the heat flux at $Ra = 5600$. It seems that the presence of a slight bimodality in the flow at $Ra \geqslant 16\,000$ and its progressive increase with further increases in the Rayleigh number explain the differences between two-dimensional and three-dimensional computations of the heat flux. Looking at figure 1 one can observe that significant discrepancies in the heat-flux computations arose and increased progressively as soon as bimodal structure of the flow pattern became more pronounced.

The analysis of successive vertical temperature profiles also gives no indication of any periodic temperature fluctuations, as was noted in the experiments by Willis & Deardorff (1967*a*) and Brown (1973). The evolution of positive and negative two-dimensional thermals was more or less steady over the range $4500 \leqslant Ra \leqslant 24\,000$. It seems that fairly discrete changes in the slope of isotherms correspond to the zones of the heat-flux transitions. Transitions in the conductive component of the heat flux support this point. The analysis of vertical and horizontal profiles shows that the transition from a two-dimensional flow pattern to a three-dimensional one occurs as soon as adjacent positive thermals near the upper boundary and negative thermals near the lower boundary merge. Figure 4 illustrates the beginning of this merging at $Ra = 24\,000$. Beyond this Rayleigh number the temperature started to be strongly periodic in both X and Y, but no fluctuations were observed until the end of the run at $Ra = 32\,000$.

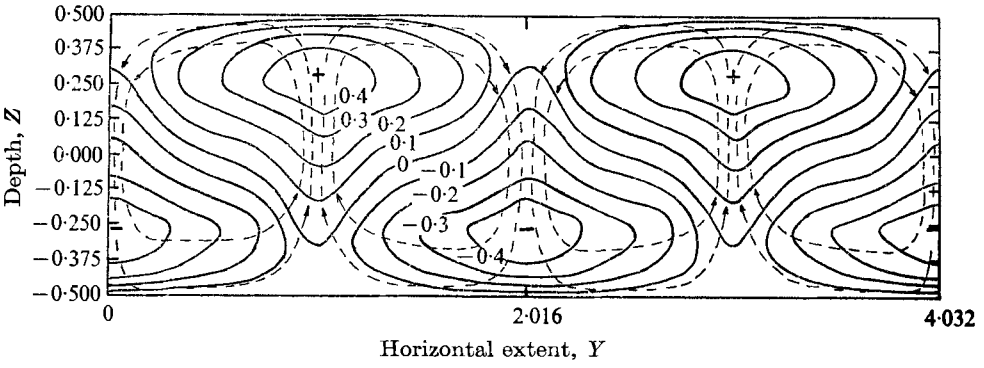

FIGURE 4. Contours of temperature deviation from the conduction profile (in non-dimensional units) across two-dimensional rolls (solid lines) at $Ra = 24000$ ($Pr = 0{\cdot}71$, $N = 0$). Streamlines are given schematically by dashed lines. Arrows indicate the direction of circulation.

There are only two differences between the numerical calculations and the experiments which might account for the above discrepancies in the flow and temperature patterns. The first is the difference in the side-wall boundary conditions and the second is the difference in the aspect ratios. Either could cause a more stable convective regime in the numerical model with cyclic side-wall boundary conditions and small aspect ratio. It is interesting, however, that the presence of oscillations in experiments does not affect such integral characteristics as the heat flux across the convective layer and the effective conductivity of the convective layer, which are quite close both in our model and in experiments with air.

Effects of Prandtl number. Numerical results for a Prandtl number $Pr = 1$ show that a rather small change in this parameter affects quantitatively the results obtained above. The non-dimensional heat flux Nu is 4–5 % larger than in the case of air. There is only one transition in the heat flux, in the range

$$10\,000 \leqslant Ra \leqslant 12\,000,$$

instead of the first and the second transitions in air. The equivalent of the third transition in air appears now in the range $16\,000 \leqslant Ra \leqslant 18\,000$.

Two-dimensional flow patterns exist over the range $4500 \leqslant Ra \leqslant 16\,000$. A weak bimodal structure appears in the flow at $Ra = 8000$, and the transition from steady quasi-two-dimensional flow to the steady three-dimensional flow takes place at $Ra = 18\,000$, together with the last transition in the heat flux.

These results disagree with the observations by Willis & Deardorff (1967*b*), which indicate that the heat-flux transitions are independent of the Prandtl number, and support the observations by Malkus (1954), which indicate transitions at $Ra \simeq 11\,000$ and $Ra \simeq 18\,000$ in acetone and water ($Pr = 3{\cdot}6$ and $6{\cdot}7$, respectively), and the observations of Krishnamurti (1970), which show transitions in both the heat flux and flow pattern at $Ra = 17\,000$ for $Pr = 6{\cdot}7$.

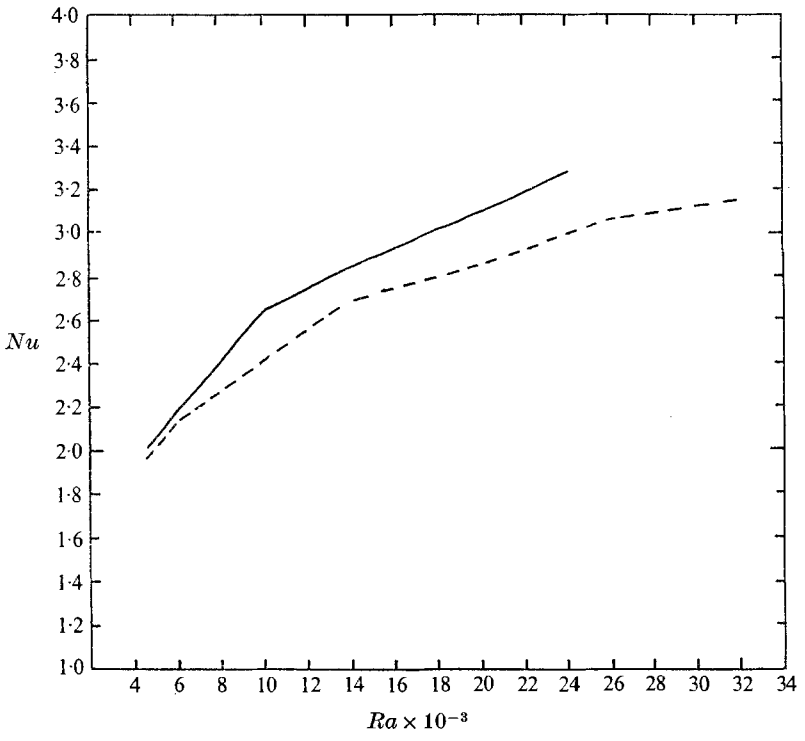

FIGURE 5. Heat flux Nu *vs.* Rayleigh number Ra for $N > 0$, $Pr = 0{\cdot}71$. Nusselt numbers for $N = 0$ are plotted for comparison (dashed line).

Nonlinear conduction temperature profile

Heat flux for $Pr = 0{\cdot}71$. A plot of the heat flux Nu *vs.* the Rayleigh number for $N > 0$ (experiment 3) is shown in figure 5. Nusselt numbers for $N = 0$ are plotted for comparison. This figure shows that the nonlinear conduction temperature profile increases the heat flux across the convective layer. The values of $\partial H/\partial Ra$ for $N > 0$ are given in table 3 together with data for $N = 0$. One can observe that the transition in the heat flux in the range $8000 \leqslant Ra \leqslant 10\,000$ for $N > 0$ corresponds to the transition in the range $24\,000 \leqslant Ra \leqslant 26\,000$ for $N = 0$.

The values of the Nusselt number for $N < 0$ are exactly the same as those in the case $N > 0$, so that the sign of the curvature of the conduction temperature profile does not affect the heat flux across the convective layer. There are, naturally, inverse distributions of the conductive and convective components of the heat flux in these two situations. Fluctuations in the heat flux appeared at $Ra = 24\,000$.

Flow and temperature pattern for $Pr = 0{\cdot}71$. Two-dimensional flow patterns were formed independently of the initial conditions at $Ra = 4500$. They differed, as at $N = 0$, only in the orientation of the rolls and the time required to obtain the final steady state. The wavelength close to the critical one was always selected. Two-dimensional rolls were stable over the range $4500 \leqslant Ra \leqslant 8000$. The main difference between these rolls and the classical ones for $N = 0$ consists of an asymmetrical horizontal distribution of upward and downward motion

$Ra \times 10^{-3}$	4·5	6	7	8	9	10	12	14	16	18	20	22	24	26	28	30	32	34	36
$N>0$	2·70				3·47							4·35							
$N=0$	2·68			2·86				3·25						3·50					

TABLE 3. Heat-flux slopes $\partial H/\partial Ra$ for $N \neq 0$ and $N = 0$ ($Pr = 0{\cdot}71$). Owing to the similarity of the heat-flux slopes for $N < 0$ and $N > 0$, only the latter are shown. Dashed lines mark the upper limits of computations.

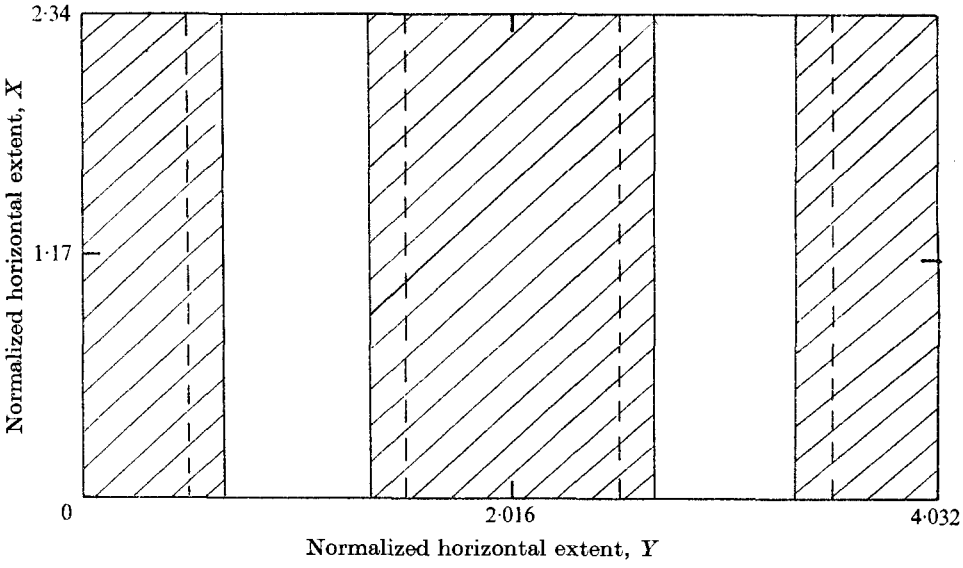

FIGURE 6. Horizontal distribution of vertical velocity in the middle of the convective layer at $Ra = 8000$ ($N > 0$, $Pr = 0{\cdot}71$). ////, areas of downward motions; ——, boundaries between ascending and descending motion for $N = 0$, plotted for comparison.

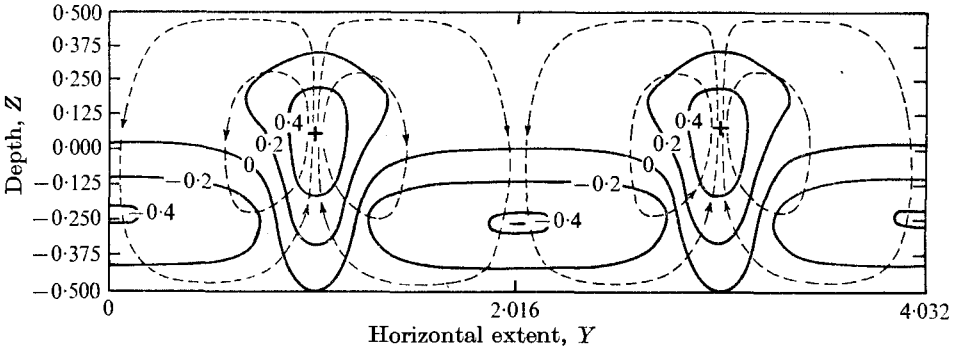

FIGURE 7. Contours of temperature deviation from the conduction profile (in non-dimensional units) across two-dimensional rolls (solid lines) at $Ra = 8000$ ($N > 0$, $Pr = 0{\cdot}71$). Schematic streamlines are indicated by dashed lines.

inside each two-dimensional cell. The area occupied by upward motion is half that occupied by downward motion when $N > 0$. The situation is reversed when $N < 0$. An example of the horizontal distribution of vertical velocity in the middle of a convective layer for $N > 0$ (experiment 3) is shown in figure 6. Asymmetry exists also in the intensity of the upward and downward motion. The intensity of the maximum vertical velocity for upward motion is twice that for downward motion when $N > 0$. This relation between the intensities is reversed when $N < 0$. An example of streamlines and the temperature distribution across such two-dimensional rolls is shown in figure 7. Comparison of this figure with figure 4 shows remarkable differences in the vertical structure of the motions and temperatures, which appear owing to the difference in the conduction temperature profiles.

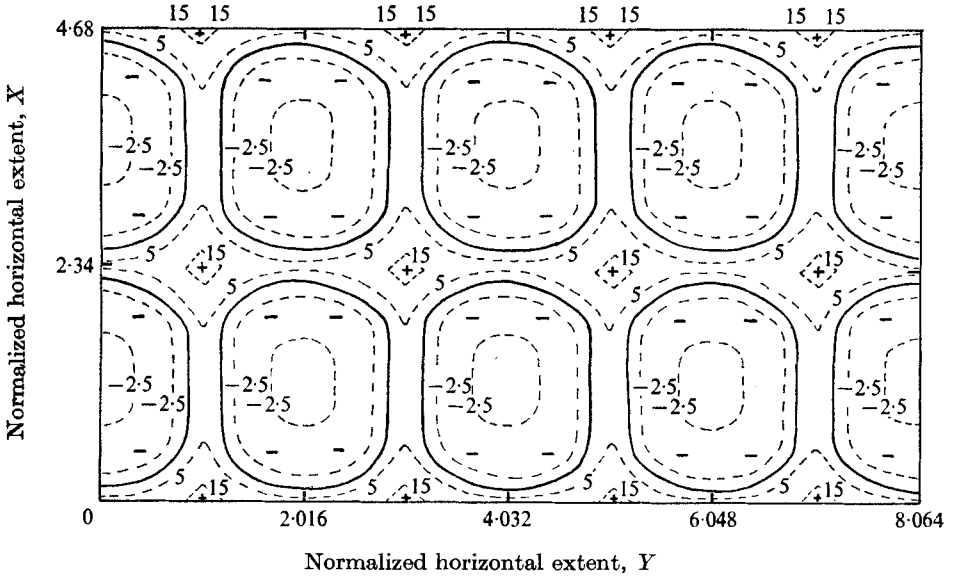

FIGURE 8. Horizontal distribution of vertical velocity near upper boundary of convective layer at $Ra = 10000$ ($N > 0$, $Pr = 0{\cdot}71$). ——, zero vertical velocity; – – –, contours of constant vertical velocity (in non-dimensional units); +, positions of maximum upward motion; −, positions of maximum downward motion. The original computational domain is repeated twice in both directions. Horizontal extents are normalized by the depth of the convective layer.

A steady three-dimensional flow pattern was formed at $Ra = 10\,000$. This transition in the flow pattern coincided with the transition in the heat flux. Figure 8 shows the horizontal distribution of vertical velocity near the upper boundary for $N > 0$. This figure shows that the flow pattern consists of large areas of descending motion bounded by narrow zones of ascending motion. The plus and minus signs in this figure correspond to the cores of regions of upward and downward motion. It is worthwhile noting that the zone of maximum descending motion is located not in the centre of the cell, but at the periphery of the area of downward motion. The intensity of the maximum vertical velocity for upward motion is approximately five times that for downward motion. The planform resembles a hexagonal one only distantly (it is intermediate between rectangular and hexagonal). It should also be noted that the vertical motions are not in phase across the convective layer at the peripheral part of the cells. Cells appear to be more rectangular near the lower boundary and more hexagonal near the upper boundary.

The motions are antisymmetric to those described above for $N < 0$. In view of the full antisymmetry of motions in the range $4500 \leqslant Ra \leqslant 8000$ for $Pr = 1$, the computations for larger Rayleigh numbers were done only for the model with $N > 0$.

At $Ra = 20\,000$ adjacent regions of downward motion merge along the X direction near the upper boundary. Time-dependent flow appears near the lower boundary, where the mean temperature gradient is largest, at $Ra = 24\,000$.

$Ra \times 10^{-3}$	4·5	6	7	8	9	10	12	14	16	18	20	22	24	26	28	30	32	34	36
$N=0$, $Pr=0{\cdot}71$	2·68			2·86				3·25						3·50					
$N=0$, $Pr=1{\cdot}0$	2·74						3·12			3·46									
$N\neq0$, $Pr=0{\cdot}71$	2·70						3·47					4·35							
$N\neq0$, $Pr=1{\cdot}0$	2·64					3·66				?									

TABLE 4. Heat-flux slopes $\partial H/\partial Ra$ for different Prandtl numbers and conduction temperature profiles. Dashed lines mark the upper limits of computations. The question mark in the last line means that the range of Rayleigh numbers after the last transition was too small to obtain a representative value of $\partial H/\partial Ra$.

Effects of Prandtl number. Computations for $Pr = 1$ show that a small change in this parameter affects quantitatively the results obtained above for air. The non-dimensional heat flux Nu is 4–5 % larger than in the case of air. Transitions in both the heat flux and flow pattern are shifted from $Ra = 10\,000$ for $Pr = 0{\cdot}71$ to $Ra = 8000$ for $Pr = 1$. An oscillatory regime near the lower boundary appears at $Ra = 20\,000$ instead of $Ra = 24\,000$ as for air.

These results support the conclusion of Thirlby (1970) that in a liquid with $Pr = 1$ two-dimensional rolls are a stable pattern at slightly supercritical Rayleigh numbers, but disagree with his conclusion that transition to three-dimensional flow takes place only for $Pr \geqslant 2{\cdot}5$.

4. Conclusions

These numerical experiments have enlarged our physical understanding of three-dimensional convection between rigid boundaries.

(i) Discrete changes in the slope of the heat-flux curve at different Rayleigh numbers are shown to be associated with changes in the flow and temperature pattern, and are dependent on the Prandtl number. These results are summarized in table 4.

(ii) Horizontally symmetric steady two-dimensional rolls and three-dimensional flow patterns exist over the range $4500 \leqslant Ra \leqslant 32\,000$ when the conduction temperature profile is linear, and horizontally asymmetric steady two-dimensional rolls and quasi-hexagonal flow patterns exist over the range

$$4500 \leqslant Ra \leqslant 20\,000$$

when the conduction temperature profile is nonlinear ($N \approx \pm 10$).

(iii) Some points still need to be clarified in view of the observational evidence of time-dependent motions instead of the steady ones obtained in this study. It should be stressed that current practical computing capabilities are only marginally adequate for the simulation of three-dimensional flows at Rayleigh numbers above 3×10^4, so that it would be highly desirable to check our results by performing similar calculations using alternative numerical methods, larger aspect ratios and finer grid resolutions.

The authors are grateful to Mr A. I. Belousov and Miss N. M. Sazanovich for their help with the computations.

REFERENCES

BROWN, W. S. 1973 Heat-flux transitions at low Rayleigh number. *J. Fluid Mech.* **60**, 539–559.

BUSSE, F. H. 1972 The oscillatory instability of convection rolls in a low Prandtl number fluid. *J. Fluid Mech.* **52**, 97–112.

CHORIN, A. J. 1968 Numerical solution of the Navier–Stokes equations. *Math. Comp.* **22**, 745–762.

KRISHNAMURTI, R. 1968*a* Finite amplitude convection with changing mean temperature. Part 1. Theory. *J. Fluid Mech.* **33**, 445–455.

KRISHNAMURTI, R. 1968*b* Finite amplitude convection with changing mean temperature. Part 2. An experimental test of the theory. *J. Fluid Mech.* **33**, 457–463.

KRISHNAMURTI, R. 1970 On the transition to turbulent convection. Part 1. The transition from two- to three-dimensional flow. *J. Fluid Mech.* **42**, 295–307.

KRISHNAMURTI, R. 1973 Some further studies on the transition to turbulent convection. *J. Fluid Mech.* **60**, 285–303.

MALKUS, W. V. R. 1954 Discrete transitions in turbulent convection. *Proc. Roy. Soc.* A **225**, 185–195.

PALM, E. 1960 On the tendency towards hexagonal cells in steady convection. *J. Fluid Mech.* **8**, 183–192.

SEGEL, L. A. 1965 The non-linear interaction of a finite number of disturbances to a layer of fluid heated from below. *J. Fluid Mech.* **21**, 359–384.

SEGEL, L. A. & STUART, J. T. 1962 On the question of the preferred mode in cellular thermal convection. *J. Fluid Mech.* **13**, 289–306.

SOMERVILLE, R. C. J. 1973 Numerical simulation of small-scale thermal convection in the atmosphere. In *Lecture Notes in Physics*, vol. 19, pp. 238–245. Springer.

THIRLBY, R. 1970 Convection in an internally heated layer. *J. Fluid Mech.* **44**, 673–693.

VELTISCHCHEV, N. F. 1969 Cellular convection in the atmosphere. *Proc. Hydrometeor. Centre USSR*,† **50**, 3–21.

VELTISHCHEV, N. F. & ŽELNIN, A. A. 1973 Numerical simulation of convection in shear flow. *Proc. Hydrometeor. Centre USSR*,† **110**, 39–47.

WILLIS, G. E. & DEARDORFF, J. W. 1967*a* Development of short-period temperature fluctuations in thermal convection. *Phys. Fluids*, **10**, 931–937.

WILLIS, G. E. & DEARDORFF, J. W. 1967*b* Confirmation and renumbering of the discrete heat flux transitions of Malkus. *Phys. Fluids*, **10**, 1861–1866.

WILLIS, G. E. & DEARDORFF, J. W. 1970 The oscillatory motions of Rayleigh convection. *J. Fluid Mech.* **44**, 661–672.

WILLIS, G. E., DEARDORFF, J. W. & SOMERVILLE, R. C. J. 1972 Roll-diameter dependence in Rayleigh convection and its effect upon the heat flux. *J. Fluid Mech.* **54**, 351–367.

† Trudy Gidrometeorologicheskogo Zentra SSSR (in Russian).